Mechanism of oil-in-liquid metal emulsion formation

Najam Ul Hassan Shah,^a Shreyas Kanetkar, ^a Aastha Uppal, ^a Michael D. Dickey, ^b Robert Y. Wang*, ^a and Konrad Rykaczewski*^{a,c}

a. School for Engineering of Matter, Transport and Energy, Arizona State University, Tempe, AZ, 85287, USA

b. Department of Chemical and Biomolecular Engineering, North Carolina State University, Raleigh, NC, 27695, USA

c. Julie Ann Wrigley Global Futures Laboratory, Arizona State University, Tempe, AZ 85287, USA

*Corresponding author emails: konradr@asu.edu, rywang@asu.edu

KEYWORDS: liquid metal foams, emulsion, oxide interface

ABSTRACT

Gallium-based liquid metals (LMs) combine metallic properties with the deformability of a liquid, which makes them promising candidates for a variety of applications. To broaden the range of physical and chemical properties, a variety of solid additives have been incorporated into the LMs within the literature. In contrast, only a handful of secondary fluids have been incorporated into LMs to create foams (gas-in-LM) or emulsions (liquid-in-LM). LM foams readily form through mixing of LM in air, facilitated by the formation of a native oxide on the LM. In contrast, LM breaks up into microdroplets when mixed with a secondary liquid such as silicone oil. Stable silicone oil-in-LM emulsions only form during mixing of the oil with LM foam. In this work, we investigate the fundamental mechanism underlying this process. We describe two possible microscale mechanisms for emulsion formation: (1) oil replacing air in the foam or (2) oil creating additional features in the foam. The associated foam-to-emulsion density difference demonstrates that emulsions predominantly form through the addition of oxide-covered silicone oil capsules into the LM foam. We demonstrate this through density and surface wettability measurements, and multiscale imaging of LM foam mixed with varied silicone oil content in air or nitrogen environments. We also demonstrate the presence of a continuous silicone oil film on the emulsion surface and that this oil film prevents the embrittlement of contacting aluminum.

INTRODUCTION

Non-toxic liquid metals (LMs) based on gallium are interesting because they have metallic properties yet are deformable like a liquid. Therefore, LMs are useful for making stretchable and soft analogs to rigid metals and have a variety of exciting prospective uses, including stretchable electronics, thermal management, biomedical, sensor, catalysis, and energy storage applications. 1-⁶ To broaden the range of physical and chemical properties, a variety of solid additives have been incorporated into the LMs, including Cu,⁷⁻¹⁰ Fe,¹⁰⁻¹² Ni,¹³⁻¹⁷ Ag,¹⁷⁻¹⁹ Mg,²⁰ Gd,²¹, BN,²⁰ W,²² SiC, 23 Cu-Fe, 24 steel, 12 diamond, 25 graphene, 26 and carbon nanotubes. 27,28 In contrast, only a handful of secondary fluids have been incorporated into LMs to create foams^{29–33} or emulsions.³⁴ These materials have been shown to have desirable characteristics, including much lower density (e.g., some foams can float on water), ^{29–33} higher adhesion, ²⁹ higher viscosity, ³⁰ and, in the case of the oil-in-LM emulsions, ³⁴ to inhibit the corrosiveness of gallium. The latter characteristic of the emulsions addresses one of the primary disadvantages of using LMs in micro-electronics, which currently necessitates expensive packaging-level methods such as introduction of corrosion barrier films. 35-38 In addition to this unique characteristic, the emulsion have a moderately high thermal conductivity of ~10 Wm⁻¹K⁻¹ that makes them uniquely suitable for high performance thermal interface materials in microelectronics applications. However, our understanding of the formation mechanisms of these fluid-in-LM materials and potential optimization routes for specific applications is only beginning to emerge.

Empirical observations have shown that the rapid formation of a thin nanoscale gallium surface oxide³⁹ enables incorporation and stabilization of gas bubbles into the LM.³⁰ These small 'capsules' permit the addition of secondary liquids such as silicone oils.³⁴ During shear mixing, the oxide that forms at the air-LM interface breaks up into microscale thin-film islands that are

continually pulled into the bulk liquid.³⁰ When the viscosity of the mixture increases sufficiently through the addition of the solids, microscale air capsules enclose in an oxide shell (created during the folding of surface waves⁴⁰) begin to be trapped within the LM. This mechanism of LM foam formation is analogous to the formation of traditional metal foams (*e.g.*, aluminum). In making these conventional materials, non-oxide particles are often added to increase the viscosity of the melted metal and mechanically stabilize internal metal-gas interfaces and bubble-bubble gaps.^{41,42}

Without the oxide formation, LM's enormous surface tension (\sim 8 times that of water), high density (\sim 6 times that of water), and low viscosity (\sim 2 times that of water) make the addition of secondary fluids challenging. For example, LM readily breaks up into micro-droplets when mixed with a similar volume of another liquid (e.g., silicone oil). $^{43-46}$ Smaller volumes of air, 47,48 silicone oil, water, peroxide, hydrochloric acid, and sodium hydroxide an be directly injected into a larger pool of LM, but rapidly escape due to large buoyancy forces. Interestingly, the environment above the LM pool can be adjusted to promote or inhibit oxide or surfactant "shell" formation, and trap either very small (\sim 5 to $10~\mu m$) or very large (\sim 1 cm) droplets of several fluids right under the external LM surface. However, these neat fluidic structures are restricted to the surface region or are temporary, and so they are of limited use in practical applications. In contrast, silicone oil with a viscosity below \sim 1000 cSt can be manually dispersed into microscale droplets (\sim 5 to 500 μ m) within LM foams to create lasting emulsions. In this work, we investigate the fundamental processes underlying the formation of these oil-in-LM emulsions.

We first describe two possible microscale mechanisms of silicone oil-in-LM emulsion formation and derive expressions for the associated density changes for the foam-to-emulsion transition that occurs as oil gets incorporated into the material. The first mechanism we discuss consists of silicone oil filling existing air pockets in the LM foam. The second mechanism we

discuss consists of silicone oil creating additional features within the LM foam. Next, we show that we can induce or inhibit oil incorporation into the LM foam by controlling the oxygen content in the environment during the LM foam and silicone oil mixing. Using density measurements, surface wettability measurements, and multiscale imaging, we elucidate how the mixing environment oxygen content alters the microscale mechanisms of the mixing process to either inhibit or enable stable emulsion formation. Lastly, we measure the thermal conductivity and aluminum corrosion inhibition characteristics to assess the potential applicability of the materials fabricated in air and nitrogen environments for microelectronics cooling applications.

EXPERIMENTAL SECTION

Materials

We purchased Gallium (Ga, 99.99% purity) and Indium (In, 99.99% purity) metals from Rotometals. We prepared the eutectic gallium indium (eGaIn) by mixing Ga and In (mass ratio of 75.5:24.5) in a glass container and heating the metals above 150 °C (melting point of Indium) for 24 hours. We allowed the prepared LM eutectic to cool to room temperature. We purchased silicone oils of different viscosities (10, 100, and 1000 cSt) and hydrogen peroxide (10 wt%) from Sigma Aldrich.

Preparation of Silicone Oil in Liquid Metal Emulsions

We fabricated the emulsions in a two-step process consisting of foam fabrication and then oil mixing.³⁴ We prepared the LM foam by shear-mixing the pure LM (eGaIn) at 600 rpm in a plastic container using an impeller.³⁰ Next, we placed 4 g of the LM foam with a controlled amount of 10 cSt silicone oil in a small plastic container and stirred the two materials manually at ~120 rpm for

30 minutes using a wooden stir rod of 1.2 mm thickness. We note that the emulsions can also be made with a faster automatic stirrer to produce materials with similar properties (see Supporting Information). We mixed the materials in either an ambient air environment or a nitrogen environment (an enclosed glove chamber that was purged and kept under positive nitrogen pressure throughout the mixing process). We note that after the mixing processes, some excess oil can remain as a shallow pool in the mixing vessel or on the mixing rod. While difficult to measure exactly, we present the estimates of actual volume of silicone oil incorporated into LM foam for each of the discussed experiments that we obtained using additional mass measurements in the Supporting Information (*i.e.*, for consistency, all silicone volume fractions presented in the main text refer to the input quantity prior to mixing). Besides the 10 cSt silicone oil, we also performed some experiments with the higher viscosity oils, which can lead to different outcomes (see Supporting Information).

Sample characterization

We used optical microscopy and cryogenic focused ion beam-scanning electron microscopy (cryo-FIB-SEM) to image the internal structure of the LM-oil samples. For optical microscopy, we cleaved the samples that were solidified in a freezer with a razor blade. We imaged the resulting large cross-sections using a Zeiss Axio Zoom.V16 microscope with Apo Z 1.5x/0 37 FWD 30 mm objective. For the microscale imaging, we used a Thermo Scientific Helios 5 UX dual beam FIB-SEM with a cryogenic transfer stage. We placed ~2 mm diameter droplets of the samples on the brass holder, which we subsequently moved into the vented and cooled transfer chamber (see step-by-step illustration of the cryogenic FIB-SEM processing and imaging procedure in the Supporting Information). Within this chamber, the sample was rapidly cooled to -150°C which freezes all its

components. Subsequently, the sample was transferred to the main microscope chamber and continually cooled throughout the rest of the characterization process. We followed our prior ion cutting and electron imaging procedure, ^{51,52} including conformal "freeze-on" deposition of an organometallic platinum protective layer onto the sample surface placing the built-in gas injection system nozzle within ~0.5 mm of the surface and then opening the nozzle for ~5 to 10 s. To make the protective coating electrically conductive, we cured this coating through exposure to high current ion beam scanning. The crude cross-sectional cuts were made with an ion beam at 30 kV and 10 to 20 nA. Subsequently, we milled smoother cross-sections in the "polishing section" mode with a lower current of 1.2 nA. We imaged the samples with 2 kV and 1.4 nA electron beam.

We measured the surface wetting properties of the foams and emulsions using a Ramé-Hart goniometer 290. We applied the LM foam or emulsion on a glass slide, flattened their upper surface using a spatula, placed the samples on the goniometer's stage, and dispensed 4 μ L droplet of deionized water onto their surface (resistance of > 14 $M\Omega cm$) using a micropipette.

We measured the thermal conductivity of eGaIn foam and silicone oil-in-LM emulsions using a thermal reference bar testing method following a modified ASTM D5470 standard. ^{53–55} For each measurement, we placed a foam or emulsion sample between two copper reference bars, sealed them using a Teflon gasket, and compressed them to about 0.01 MPa and a 2 mm thickness. Further specifics of this measurement are described in depth in our prior work. ⁵⁵

We measured the density of each eGaIn foam or emulsion sample using the Archimedes principle.^{30,34} Specifically, we molded and solidified each sample into a small block (\sim 1 cm x \sim 1 cm x \sim 0.5 cm) and suspended it in a small beaker filled with water placed over a micro-balance.

RESULTS AND DISCUSSION

Two mechanisms of liquid-in-LM emulsions formation

In principle, liquid-in-LM emulsions can be formed through the incorporation of the secondary liquid into the LM foam via the two routes illustrated in Figure 1. First, the secondary liquid could replace the air inside existing features within the foam (see Figure 1a). In this "replacement mechanism", the secondary liquid fills open-cell features such as pores (see Figure 1b), but also could replace air within capsules ruptured at the foam-secondary liquid interface during mixing (see Figure 1c). Second, additional gallium oxide-enclosed secondary liquid closed-cell features ("capsules") can form during the perturbation of the oxide at the two bulk fluid interfaces throughout the mixing process (see Figure 1d and 1e). This "addition mechanism" of secondary liquid requires the continual formation of oxide at the two bulk fluids interface. Some oxide regrowth could also be needed to seal ruptured capsules in which secondary liquid replaced the air. As for foams, the mechanical stabilization of the emulsions requires the presence of oxide fragments or potentially other solid particles within the LM that prevent the buoyancy-driven escape of secondary liquid by bridging the space between capsules. Next, we derive expressions for the expected density of the emulsions and show that the predominant mechanism by which secondary liquid incorporates into the LM foam can be distinguished from the foam-to-emulsion density change.

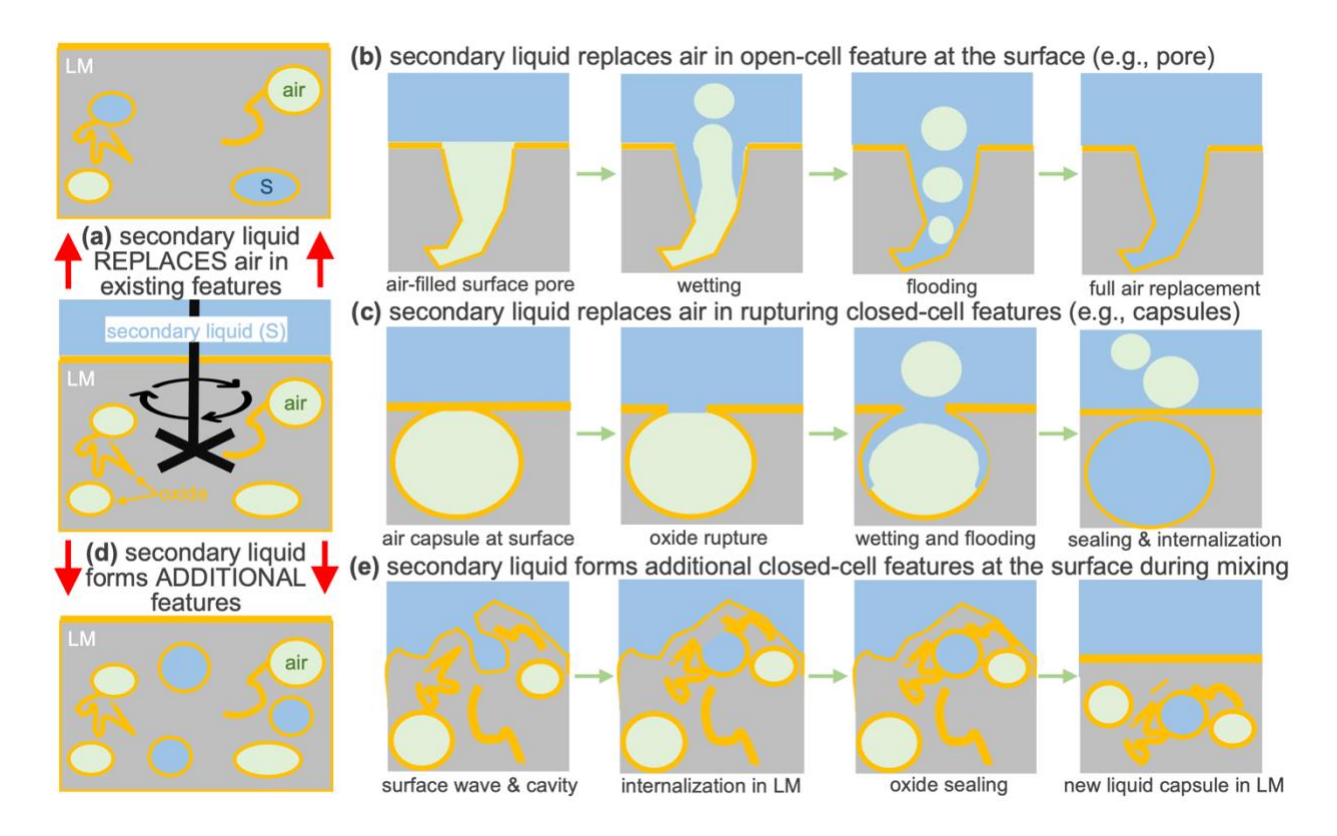


Figure 1. Schematics of possible emulsion formation mechanism consisting of (a) air replacement by the secondary liquid (S) in (b) open-cell LM foam geometrical features such as pores at the surfaces or (c) closed-cell features such as air capsules that temporarily rupture at the surfaces during mixing and alternatively (d) secondary liquid forming additional closed-cell geometrical features in LM foam such as (e) capsules formed by surface wave cresting to form secondary liquid-filled cavities that seal into new features with regrown oxide.

Theoretical LM foam-to-emulsion density difference for the two emulsion formation mechanisms

The density of the LM foam, ρ_f , can be expressed with volumes and densities of its components as:

$$\rho_f = \frac{V_a \rho_a + V_{LM} \rho_{LM} + V_{ox} \rho_{ox}}{V_a + V_{LM} + V_{ox}} \tag{1}$$

Where V is the volume and ρ the density of the air (subscript a), liquid metal (subscript LM), and oxide (subscript ox) components. For the specific case in this work, the density of the LM oxide and the LM are nearly identical ($\rho_{LM} \approx \rho_{ox} \approx 6 \text{ g cm}^{-3}$), we can rewrite **Eq.1** as:

$$\rho_f = \frac{V_a \rho_a + (V_{LM} + V_{OX}) \rho_{LM}}{V_a + V_{LM} + V_{OX}} \tag{2}$$

In addition, the oxide is only present in ~1 to 3 nm thick films, 56,57 so the volume it occupies is much smaller than that of the LM or air (i.e., $V_{ox} \ll V_{LM}$ and $V_{ox} \ll V_a$). Accordingly, we simplify the analysis by assuming that we can neglect the oxide volume:

$$\rho_f \approx \frac{V_a \rho_a + V_{LM} \rho_{LM}}{V_a + V_{LM}} \tag{3}$$

If the secondary liquid with density ρ_s is incorporated into the LM foam purely through the air replacement mechanism (**Figure 1a-c**), there should be either no change or a very minor change in the total volume during the process. In other words, we can assume that the secondary liquid volume (V_s) replaces some fraction of the air volume present in the foam (V_a), which leads to a reduced air volume (V_a^*) within the emulsion ($V_a^* = V_a - V_s$). As such, the density of the emulsion formed with the air replacement mechanisms is (ρ_{e-r}):

$$\rho_{e-r} = \frac{V_a^* \rho_a + V_{LM} \rho_{LM} + V_s \rho_s}{V_a^* + V_{LM} + V_s} = \frac{(V_a - V_s) \rho_a + V_{LM} \rho_{LM} + V_s \rho_s}{V_a - V_s + V_{LM} + V_s} = \frac{V_a \rho_a + V_{LM} \rho_{LM} + V_s (\rho_s - \rho_a)}{V_a + V_{LM}}$$
(4)

Combining **Eq. 3** and **Eq.4**, we obtain:

$$\rho_{e-r} = \frac{V_a \rho_a + V_{LM} \rho_{LM}}{V_a + V_{LM}} + \frac{V_s (\rho_s - \rho_a)}{V_a + V_{LM}} = \rho_f + \frac{V_s (\rho_s - \rho_a)}{V_a + V_{LM}} = \rho_f + \phi_s^* (\rho_s - \rho_a)$$
 (5)

where $\phi_s^* = V_s/(V_a + V_{LM}) = V_s/(V_a^* + V_{LM} + V_s)$ is the volume fraction of the secondary liquid in the emulsion formed through the replacement mechanism.

On the other hand, if the secondary liquid (assumed to be incompressible) is incorporated into the LM foam purely through the addition mechanism, the total volume of the resulting emulsion will be higher than that of the input foam by a factor of $\lambda = (V_a + V_{LM} + V_s)/(V_a + V_{LM})$. This

factor can be expressed in terms of the volume fraction of secondary liquid in the addition mechanism (ϕ_s) as $\lambda^{-1} = (V_a + V_{LM})/(V_a + V_{LM} + V_s) = 1 - V_s/(V_a + V_{LM} + V_s) = 1 - \phi_s$. As such, the density of the emulsion formed with the secondary liquid addition mechanisms (ρ_{e-a}) is:

$$\rho_{e-a} = \frac{v_a \rho_a + v_{LM} \rho_{LM} + v_s \rho_s}{v_a + v_{LM} + v_s} = \frac{v_a \rho_a + v_{LM} \rho_{LM} + v_s \rho_s}{\lambda (v_a + v_{LM})} = \lambda^{-1} \frac{v_a \rho_a + v_{LM} \rho_{LM} + v_s \rho_s}{v_a + v_{LM}}$$
(6)

Combining **Eq. 3** and **Eq.6**, we obtain:

$$\rho_{e-a} = \lambda^{-1} \left[\frac{V_a \rho_a + V_{LM} \rho_{LM}}{V_a + V_{LM}} + \frac{V_s \rho_s}{V_a + V_{LM}} \right] = \lambda^{-1} \left[\rho_f + \rho_s \frac{\{V_s + V_a + V_{LM} - (V_a + V_{LM})\}}{V_a + V_{LM}} \right]$$
(7)

Through algebraic manipulation and substitution of the definition of λ , we can simplify **Eq.7** to:

$$\rho_{e-a} = \lambda^{-1} [\rho_f + (\lambda - 1)\rho_s] = (1 - \phi_s)\rho_f + \phi_s \rho_s = \rho_f - \phi_s (\rho_f - \rho_s)$$
 (8)

The derived **Eq.5** and **Eq.8** demonstrate that the two secondary liquid incorporation mechanisms have an opposing impact on the foam-to-emulsion density change. Specifically, since any secondary liquid is denser than air $(\rho_s > \rho_a)$, emulsions formed under the air replacement mechanism will always be denser than the original foam (*i.e.*, $\rho_{e-r} > \rho_f$ for $\phi_s > 0$). In contrast, when the LM foam is denser than the secondary liquid ($\rho_s < \rho_f$ as for silicone oil and our foams), emulsions formed through the addition mechanism will be lighter than the original foam (*i.e.*, $\rho_f > \rho_{e-a}$ for $\phi_s > 0$). Furthermore, both the positive and negative density difference ($\rho_{e-r} - \rho_f$ or $\rho_{e-a} - \rho_f$) should be proportional to the volume fraction of incorporated secondary liquid in the emulsion. Next, we experimentally explore the two fluid mixing processes and compare the results against our analytical predictions.

The density of silicone oil and LM foam mixed in air and nitrogen environments

We manually mixed 10 cSt silicone oil and eGaIn foam for 30 minutes in either air³⁴ or nitrogen environments (see **Figure 2a-b**). As expected, mixing within an air environment leads to the incorporation of all the oil into the LM foam and formation of a stable silicone oil-in-LM emulsion (see **Figure 2a**).³⁴ Oxide shell formation at silicone oil and LM interface in air environment has been previously observed,⁴⁸ and is likely promoted by continual replenishment of oxygen near the interface during mixing. In contrast, we visually did not observe any silicone oil mixing into the LM foam in a nitrogen environment (see **Figure 2b**). In more quantitative terms, the measurements in **Figure 2c** show that the density of the LM foam after mixing with any volume fraction of silicone oil in a nitrogen environment is only 0.1 to 0.3 g cm⁻³ (2 to 6%) higher than that of the original foam. Similarly, the density of the LM emulsion (*i.e.*, silicone oil and LM foam mixed in an air environment) with only a 10% oil input volume fraction is about the same as that of the original foam. However, with more silicone oil added, the density of the emulsion decreases linearly with the secondary liquid's input fraction. For the 40:60 input volume ratio between the silicone oil and LM foam, the emulsion density is ~1 g cm⁻³ (20%) lower than the original foam.

The linear decrease of the emulsion density with increasing input oil volume fraction past the 10% threshold agrees with **Eq.8** predictions. This observation provides support for the occurrence of the secondary liquid addition emulsion formation mechanism (**Figure 1d-e**). In the case of the fluid mixing in nitrogen, the lack of oxygen in the environment likely prevents the continual growth of an oxide shell that is critical to the stability of the new silicone oil capsules. To provide further evidence that the lack of oxide growth prevents stable silicone oil capsule formation, we mixed an "oxide forming" liquid (hydrogen peroxide)⁴⁸ with the LM foams in both environments. In other words, we decoupled the oxide-shell formation from the mixing environment oxygen content. Confirming that oxide growth is necessary for the silicone oil capsule stability, the

hydrogen peroxide was incorporated into the LM foam in both environments (see Supporting Information for example experiment).

Oxide growth prevention could also inhibit the silicone oil from replacing air in rupturing capsules because they could not be re-sealed (see **Figure 1d**). However, the data trend agreement between the density measurements and **Eq. 8** indicates that the air replacement mechanism does not occur for geometrical features within the bulk of the foam. This observation allows us to propose an explanation for the minor density increase when mixing oil and the LM foam in nitrogen and when mixing small (i.e., 10%) silicone oil volume fractions with the LM foam in air. Specifically, in both cases, the silicone oil likely replaces air within "open-cell" features on the foam surface. Since these open-cell features are only present on the surface, they are limited in number, and their filling leads to a much smaller density change than the addition of the much more abundant oil capsules. Next, we provide further evidence for our explanation of the density measurements using surface wettability measurements and multiscale imaging.

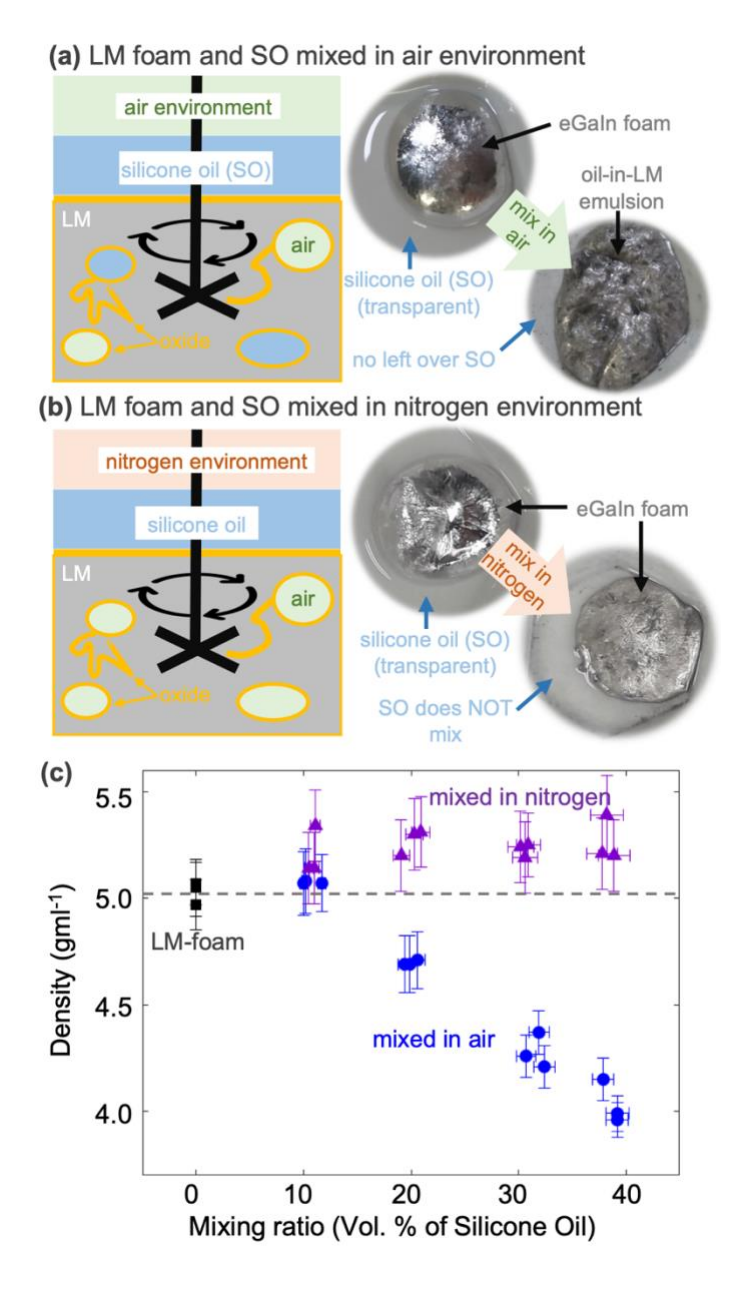


Figure 2. Schematics and example images of LM foam and silicone oil (SO) mixing in (a) an air (i.e., the emulsion) and (b) nitrogen environment; (c) the density of the LM materials resulting from the two mixing processes with varying input volumetric ratios of SO and LM foam.

Surface wettability and multiscale imaging of the silicone oil mixed with the LM foam in air and nitrogen environments

The presence of silicone oil on the surface of the LM foam or emulsion strongly impacts the surface water contact angle. In particular, the plot in **Figure 3** shows that while the LM foams are hydrophilic with contact angles varying from about 10° to 40°, the emulsions are nearly or slightly hydrophobic with contact angles of about 80° to 95°. The substantial increase of the water contact angle with the silicone oil addition implies that the oil forms a continuous surface. The resulting hybrid solid-liquid surface is analogous to oil-impregnated surfaces. In contrast, the water droplets placed on the surface of the LM foam mixed with silicone oil in the nitrogen environment have contact angles varying greatly between 35° to 90°. This observation implies that mixing the foam and silicone oil in the nitrogen environments leads to only partial coverage of the LM foam surface by the silicone oil. Next, we explore the surface and cross-sectional morphology of these materials using multiscale imaging.

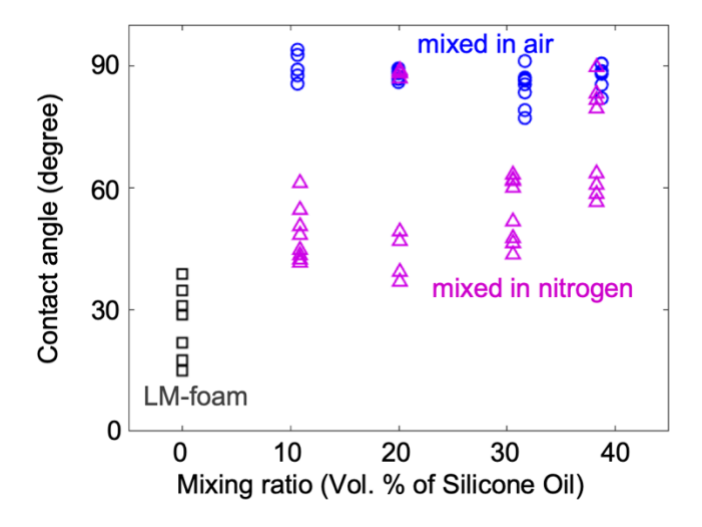


Figure 3. Water contact angles measured on the surfaces of the LM foam and its mixtures with silicone oil made in an air (*i.e.*, emulsion) or nitrogen environment as a function of the silicone oil and the LM foam volumetric mixing ratio.

Figure 4 presents optical and cryo-FIB-SEM surface and cross-sectional images of the bare LM foam (**a**) as well as LM foam mixed with silicone oil in nitrogen (**b**) and air (**c**) environments. The LM foam contains 100 nm to 200 μm air capsules and has various surface features, including multiscale wrinkles^{39,58} and 5 μm to 100 μm "open-cell" pores. While the cross-sectional optical image of the LM foam mixed with silicone oil in nitrogen is indistinguishable from that of the original LM foam (**Figure 4a** and **4b**), the presence of oil capsules is clearly visible in the emulsion cross-section (**Figure 4c**). The amount of internal silicone oil features visible in the cross-sections within these emulsions increases with the mixing ratio of the two fluids (see Supporting Information).

The electrically insulating nature of the silicone oil facilitates its identification in surface electron micrographs of the cryogenically frozen samples. Upon exposure to the electron beam, the oil surface charges and deflects incoming electrons creating dull-gray to bright-white colors and streaky image sections. ^{52,59} With this "lens", we can easily interpret from the electron micrographs that the surface of the emulsions is covered by a continuous oil film that is only pierced by occasional "islands" of locally elevated LM foam topology. In contrast, the surface of the materials mixed in the nitrogen environment is covered by "puddles" of silicone oil and occasional oil-filled pores. The corresponding sample's near-surface cross-sections exposed using ion beam milling confirm observations from exterior surface imaging. Furthermore, the cross-sectional images show that the silicone oil puddles are very shallow, with a thickness of about 100 nm. In comparison, the continuous liquid film is several times thicker (about 300 to 500 nm).

The measured linear decrease in density with mixing volume fraction of silicone oil that was predicted by **Eq.8** and the presence of silicone oil in the cross-sectional images provide strong evidence that the emulsions form through incorporation of additional, oxide-covered, liquid

capsules. New oxide growth is limited without oxygen in the mixing environment, preventing stable silicone oil capsules and emulsion from forming in nitrogen. Thus, when mixed with the LM foam in nitrogen, the silicone oil only forms puddles and fills exposed pores on the exterior surface. The minor 5 to 10% density increase is independent of the silicone oil to LM foam mixing ratio in the nitrogen environment because even a small volume of the oil saturates the limited surface features of the foam. We suspect that in a nitrogen environment, the silicone oil only fills pores and forms puddles on the surface because the lack of oxygen prevents the formation of oxide wrinkles on the LM surface (i.e., oil interacts with a smooth exterior surface). Such nanoscale and microscale wrinkles readily form on LM surface even the samples are lightly disturbed in lab environment.^{39,58} The motion (or mixing) induced tension on the exterior LM surface likely creates temporary oxide shell micro-fractures that quickly turn into additional oxide film. Since the new oxide surface area is larger than the original but the volume of the liquid remain effectively unchanged, the oxide surface buckles and wrinkles on multiple length scales. The lack or only trace oxygen content in the nitrogen atmosphere is not sufficient to promote ample formation of such surface texture. In contrast, during mixing with oil in air, the surface waves on the LM surface are preserved in multiscale wrinkles. Since oxide shell forms on the post-mixing surface of the LM foam mixed in nitrogen environment either from trace oxygen content or once the sample is placed in air, it is most likely the highly textured surface of the emulsion mixed in air that supports the continuous silicone oil film formation (vs. partial dewetting into puddles).

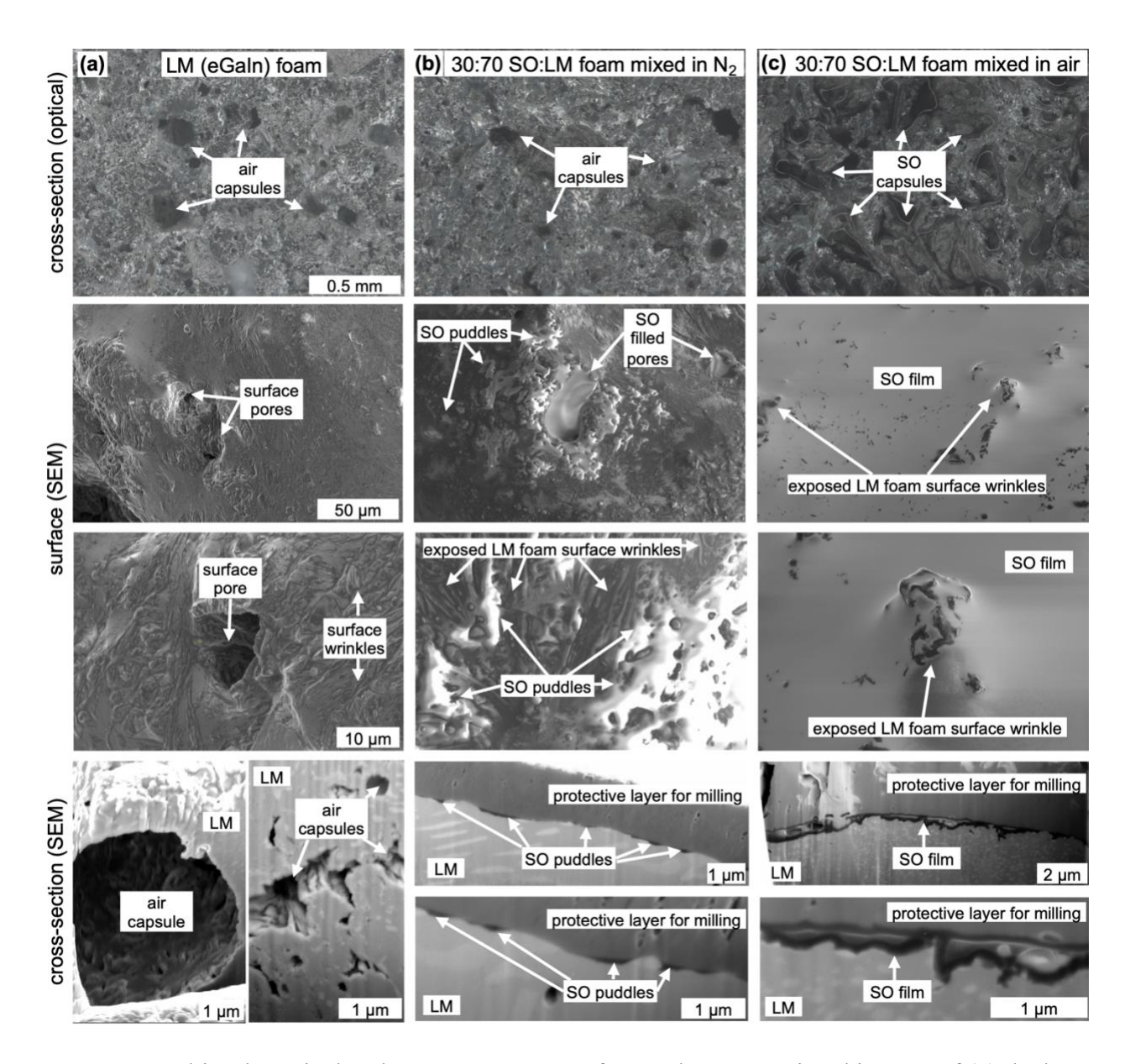


Figure 4. Multiscale optical and cryo-FIB-SEM surface and cross-sectional images of (a) the bare LM foam and (b & c) the LM foam mixed with silicone oil (SO) in (b) nitrogen and (c) air environments.

Suitability of the silicone oil and LM foam mixtures mixed in the air and nitrogen environment for thermal interface materials: thermal conductivity and aluminum corrosion inhibition

Due to their high thermal conductivity and conformability, LMs are increasingly being used as thermal interface materials (TIMs) within the microelectronics industry. However, gallium-based LMs induce corrosion or embrittlement to most metals, 60,61 which requires costly deposition of protective barrier films for LM TIM implementation. Potentially resolving this issue, we previously demonstrated that silicone oil-in-gallium foam emulsion (10 cSt with 40% silicone oil) does not embrittle aluminum while at the same time exhibits a moderately high thermal conductivity of about 10 W m⁻¹ K⁻¹. The current emulsions with the same 10 cSt silicone oil fraction (made with eGaIn, not pure gallium foam) also do not corrode the foils (see photographs of aluminum foils before and after 24 hour compression against the LM-based materials in Supporting Information). The cryo-FIB-SEM images confirm our prior hypothesis that the surface of the emulsions is covered by a continuous layer of silicone oil, which prevents direct LM-aluminum contact. In contrast, such contact and ensuing embrittlement of aluminum are not prevented by the silicone oil puddles on the surface of the materials mixed in a nitrogen environment.

From a thermal perspective, the conductivity of the emulsions are similar to our prior results.³⁴ In particular, the emulsion effective thermal conductivity steadily decreases with increased silicone oil volume fraction (see **Figure 5**). The effective thermal conductivity of the materials accounts for the intrinsic (*i.e.*, bulk) thermal conductivity of the material as well as for the thermal contact resistances of the two sample-measurement bar interfaces.⁵⁵ Consequently, we attribute the observed decrease in the effective thermal conductivity to the low thermal conductivity microcapsules (~0.2 to 0.3 W m⁻¹ K⁻¹),⁴³ whose number increases as the silicone oil volume fraction

increases. In contrast, the effective thermal conductivity of the LM foam mixed with silicone oil in nitrogen environments is comparable to or even slightly higher than that of the bare LM foam (around 18 Wm⁻¹K⁻¹). This minor effective thermal conductivity increase might stem from the thermal contact resistance reduction by the exterior silicone oil puddles. The continuous silicone oil film on the surface of the emulsions likely also induces a similar or even more significant thermal contact resistance reduction. However, this benefit is negated by decreased intrinsic thermal conductivity associated with silicone oil capsule addition. Consequently, for thermal management applications, the LM foams mixed with silicone oil in a nitrogen environment do not provide any major benefits over bare LM foams. In contrast, the use of the emulsions could remove the need for protective barrier layers, albeit at the cost of reduced thermal conductivity.

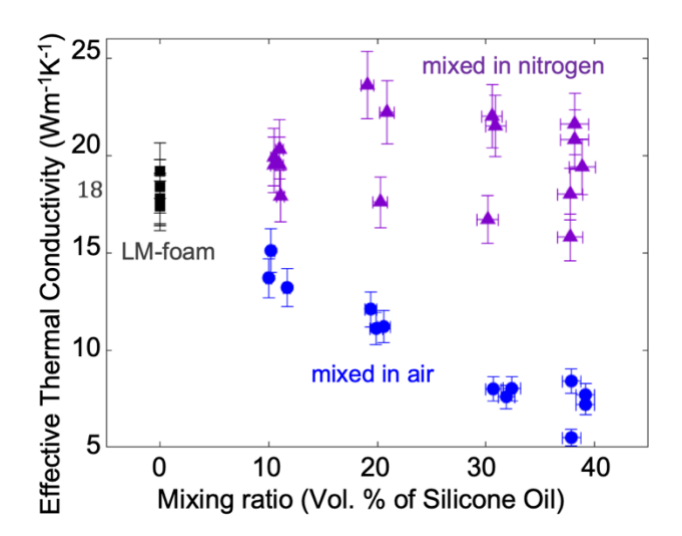


Figure 5. The effective thermal conductivity the bare LM foam and the LM foam mixed with silicone oil in nitrogen and air (i.e., the emulsions) environments.

CONCLUSION

In summary, we described two possible mechanisms for the formation of silicone oil-in-LM emulsions and theoretically demonstrated that the dominant mechanism can be distinguished through foam-to-emulsion density change. Specifically, we described the "replacement mechanism" that consists of silicone oil replacing air features in the LM foam and the "addition mechanism" that consists of silicone oil creating additional features within the LM foam. We theoretically demonstrated that the former mechanism should be associated with a linear increase in the emulsion density with increasing silicone oil mixing volume fraction, while the latter mechanism should have the opposite effect.

Our measurements showed that past the 10% oil volume fraction threshold, the density of the emulsions decreases linearly with increasing the silicone oil content. Using multiscale imaging and wettability measurements, we confirmed that mixing the silicone oil and LM foam in air leads to the incorporation of silicone oil capsules and the formation of emulsions. Consequently, the silicone oil-in-LM emulsions predominantly form by the addition of new silicone oil capsules, as opposed to the replacement of air by the oil in existing foam features.

We also demonstrated that when silicone oil and LM foam are mixed in a nitrogen environment, there is a small increase in the resulting material density that is independent of the oil volume fraction. By removing oxygen from the mixing environment, we prevented the growth of oxide shell on the oil capsules, which is critical for silicone oil incorporation into the bulk material. Without the oxide growth, cryo-FIB-SEM images revealed that the silicone oil only replaces air within open-cell surface features (*e.g.*, micro-pores) and forms ~100 nm deep puddles on the LM foam surface. The process leads to a small density increase that is independent of the added volume of silicone oil because there is a limited number of open-cell surface features that

are easily saturated by the oil. Interestingly, the surface of the emulsion is covered by a thicker (~300 to 500 nm) and continuous silicone oil film. Its presence explains the lack of density decrease that we observed for the 10% silicone oil volume fraction (i.e., density increases because of the replacement of air in surface features, but its increase is counterbalanced by the addition of silicone capsules into the bulk of the material). We suspect that mixing of the two fluids in air allows a continuous exterior silicone oil film to form because it promotes continual formation and preservation of multiscale oxide wrinkles. These surface textures do not form on the LM surface during mixing in a nitrogen environment, leading to local dewetting of the silicone oil film. Lastly, we showed that the continuous silicone oil film on the emulsion surface is necessary to prevent LM-induced embrittlement of contacting aluminum. This unique feature of the silicone oil-in-LM emulsions makes them potential candidates for thermal management applications.

ASSOCIATED CONTENT

Supporting Information The Supporting Information is available free of charge on the ACS Publications website. Silicone oil-in-LM formation using high speed stirring, plot of actual silicone oil volume internalized in the LM foam, effect of silicone oil viscosity on mixing with LM foam in nitrogen, results of peroxide mixing with LM foam in air and nitrogen, additional cross-sectional images of emulsions made with varied silicone oil content, and aluminum embrittlement results are discussed.

AUTHOR INFORMATION

Corresponding Author

*email: konradr@asu.edu and rywang@asu.edu

Author Contributions

The manuscript was written through contributions of all authors. All authors have given approval to the final version of the manuscript.

Funding Sources

This research was funded by National Science Foundation Division of Civil, Mechanical and Manufacturing Innovation grant 2032415. NUHS was supported by the Fulbright-HEC Scholarship program.

ACKNOWLEDGMENT

The authors gratefully acknowledge the use of the microscopy equipment within the LeRoy Eyring Center for Solid State Science at Arizona State University.

REFERENCES

(1) Daeneke, T.; Khoshmanesh, K.; Mahmood, N.; de Castro, I. A.; Esrafilzadeh, D.; Barrow, S. J.; Dickey, M. D.; Kalantar-Zadeh, K. Liquid Metals: Fundamentals and Applications in Chemistry. *Chem Soc Rev* **2018**, *47* (11), 4073–4111.

- (2) Chen, S.; Wang, H.-Z.; Zhao, R.-Q.; Rao, W.; Liu, J. Liquid Metal Composites. *Matter* **2020**, 2 (6), 1446–1480.
- (3) Malakooti, M. H.; Bockstaller, M. R.; Matyjaszewski, K.; Majidi, C. Liquid Metal Nanocomposites. *Nanoscale Adv* **2020**, *2* (7), 2668–2677.
- (4) Chen, S.; Deng, Z.; Liu, J. High Performance Liquid Metal Thermal Interface Materials. *Nanotechnology* **2020**, *32*, 092001. https://doi.org/10.1088/1361-6528/abcbc2.
- (5) Lu, Y.; Hu, Q.; Lin, Y.; Pacardo, D. B.; Wang, C.; Sun, W.; Ligler, F. S.; Dickey, M. D.; Gu, Z. Transformable Liquid-Metal Nanomedicine. *Nat Commun* **2015**, *6*.
- (6) Handschuh-Wang, S.; Stadler, F. J.; Zhou, X. Critical Review on the Physical Properties of Gallium-Based Liquid Metals and Selected Pathways for Their Alteration. *The Journal of Physical Chemistry C* 2021, 125 (37), 20113–20142.
- (7) Li, G.; Ji, Y.; Wu, M.; Ma, H. Highly Conductive Thermal Paste of Liquid Metal Alloy Dispersed with Copper Particles. In *Proceedings of the ASME 2016 heat transfer summer conference*; Wahington DC, 2016.
- (8) Tang, J.; Zhao, X.; Li, J.; Guo, R.; Zhou, Y.; Liu, J. Gallium-Based Liquid Metal Amalgams: Transitional-State Metallic Mixtures (TransM2ixes) with Enhanced and Tunable Electrical, Thermal, and Mechanical Properties. *ACS Appl Mater Interfaces* **2017**, *9* (41), 35977–35987. https://doi.org/10.1021/acsami.7b10256.
- (9) Ralphs, M. I.; Kemme, N.; Vartak, P. B.; Joseph, E.; Tipnis, S.; Turnage, S.; Solanki, K. N.; Wang, R. Y.; Rykaczewski, K. In Situ Alloying of Thermally Conductive Polymer Composites by Combining Liquid and Solid Metal Microadditives. *ACS Appl Mater Interfaces* **2018**, *10* (2), 2083–2092. https://doi.org/10.1021/acsami.7b15814.
- (10) Tutika, R.; Zhou, S. H.; Napolitano, R. E.; Bartlett, M. D. Mechanical and Functional Tradeoffs in Multiphase Liquid Metal, Solid Particle Soft Composites. *Adv Funct Mater* **2018**, *28* (45), 1804336. https://doi.org/10.1002/adfm.201804336.
- (11) Ren, L.; Sun, S.; Casillas-Garcia, G.; Nancarrow, M.; Peleckis, G.; Turdy, M.; Du, K.; Xu, X.; Li, W.; Jiang, L.; Dou, S. X.; Du, Y. A Liquid-Metal-Based Magnetoactive Slurry for Stimuli-Responsive Mechanically Adaptive Electrodes. *Advanced Materials* **2018**, *30* (35), 1802595. https://doi.org/10.1002/adma.201802595.
- (12) Carle, F.; Bai, K.; Casara, J.; Vanderlick, K.; Brown, E. Development of Magnetic Liquid Metal Suspensions for Magnetohydrodynamics. *Phys Rev Fluids* **2017**, *2* (1), 013301. https://doi.org/10.1103/PhysRevFluids.2.013301.
- (13) Guo, R.; Wang, X.; Chang, H.; Yu, W.; Liang, S.; Rao, W.; Liu, J. Ni-Galn Amalgams Enabled Rapid and Customizable Fabrication of Wearable and Wireless Healthcare Electronics. *Adv Eng Mater* **2018**, *20* (10), 1800054.
- (14) Wang, X.; Guo, R.; Yuan, B.; Yao, Y.; Wang, F.; Liu, J. Ni-Doped Liquid Metal Printed Highly Stretchable and Conformable Strain Sensor for Multifunctional Human-Motion Monitoring. In 2018 40th Annual International Conference of the IEEE Engineering in Medicine and Biology Society (EMBC); IEEE, 2018; pp 3276–3279.
- (15) Ralphs, M.; Kong, W.; Wang, R. Y.; Rykaczewski, K. Thermal Conductivity Enhancement of Soft Polymer Composites through Magnetically Induced Percolation and Particle—Particle Contact Engineering. Adv Mater Interfaces 2019, 6 (6), 1801857. https://doi.org/10.1002/admi.201801857.

- (16) Daalkhaijav, U.; Yirmibesoglu, O. D.; Walker, S.; Mengüç, Y. Rheological Modification of Liquid Metal for Additive Manufacturing of Stretchable Electronics. *Adv Mater Technol* 2018, 3 (4), 1700351. https://doi.org/10.1002/admt.201700351.
- (17) Tang, J.; Zhao, X.; Li, J.; Zhou, Y.; Liu, J. Liquid Metal Phagocytosis: Intermetallic Wetting Induced Particle Internalization. *Advanced Science* **2017**, *4* (5), 1700024. https://doi.org/10.1002/advs.201700024.
- (18) Lin, Z.; Liu, H.; Li, Q.; Liu, H.; Chu, S.; Yang, Y.; Chu, G. High Thermal Conductivity Liquid Metal Pad for Heat Dissipation in Electronic Devices. *Appl Phys A Mater Sci Process* **2018**, 124 (5), 368. https://doi.org/10.1007/s00339-018-1778-z.
- (19) Tavakoli, M.; Malakooti, M. H.; Paisana, H.; Ohm, Y.; Green Marques, D.; Alhais Lopes, P.; Piedade, A. P.; de Almeida, A. T.; Majidi, C. EGaln-Assisted Room-Temperature Sintering of Silver Nanoparticles for Stretchable, Inkjet-Printed, Thin-Film Electronics. *Advanced Materials* **2018**, *30* (29), 1801852. https://doi.org/10.1002/adma.201801852.
- (20) Wang, X.; Yao, W.; Guo, R.; Yang, X.; Tang, J.; Zhang, J.; Gao, W.; Timchenko, V.; Liu, J. Soft and Moldable Mg-Doped Liquid Metal for Conformable Skin Tumor Photothermal Therapy. *Adv Healthc Mater* **2018**, *7* (14), 1800318. https://doi.org/10.1002/adhm.201800318.
- (21) De Castro, I. A.; Chrimes, A. F.; Zavabeti, A.; Berean, K. J.; Carey, B. J.; Zhuang, J.; Du, Y.; Dou, S. X.; Suzuki, K.; Shanks, R. A.; Nixon-Luke, R.; Bryant, G.; Khoshmanesh, K.; Kalantar-Zadeh, K.; Daeneke, T. A Gallium-Based Magnetocaloric Liquid Metal Ferrofluid. *Nano Lett* **2017**, *17* (12), 7831–7838. https://doi.org/10.1021/acs.nanolett.7b04050.
- (22) Kong, W.; Wang, Z.; Wang, M.; Manning, K. C.; Uppal, A.; Green, M. D.; Wang, R. Y.; Rykaczewski, K. Oxide-Mediated Formation of Chemically Stable Tungsten–Liquid Metal Mixtures for Enhanced Thermal Interfaces. *Advanced Materials* **2019**, *31* (44). https://doi.org/10.1002/adma.201904309.
- (23) Kong, W.; Wang, Z.; Casey, N.; Korah, M. M.; Uppal, A.; Green, M. D.; Rykaczewski, K.; Wang, R. Y. High Thermal Conductivity in Multiphase Liquid Metal and Silicon Carbide Soft Composites. *Adv Mater Interfaces* **2021**, 2100069.
- (24) Li, F.; Kuang, S.; Li, X.; Shu, J.; Li, W.; Tang, S.; Zhang, S. Magnetically-and Electrically-Controllable Functional Liquid Metal Droplets. *Adv Mater Technol* **2019**, *4* (3), 1800694.
- (25) Wei, S.; Yu, Z.; Zhou, L.; Guo, J. Investigation on Enhancing the Thermal Conductance of Gallium-Based Thermal Interface Materials Using Chromium-Coated Diamond Particles. *Journal of Materials Science: Materials in Electronics* **2019**, *30* (7), 7194–7202. https://doi.org/10.1007/s10854-019-01038-0.
- (26) Sargolzaeiaval, Y.; Ramesh, V. P.; Neumann, T. V.; Miles, R.; Dickey, M. D.; Öztürk, M. C. High Thermal Conductivity Silicone Elastomer Doped with Graphene Nanoplatelets and Eutectic Galn Liquid Metal Alloy. *ECS Journal of Solid State Science and Technology* **2019**, 8 (6), P357–P362. https://doi.org/10.1149/2.0271906jss.
- (27) Ma, K. Q.; Liu, J. Nano Liquid-Metal Fluid as Ultimate Coolant. *Physics Letters, Section A* **2007**, *361* (3), 252–256. https://doi.org/10.1016/j.physleta.2006.09.041.
- (28) Zhao, L.; Chu, S.; Chen, X.; Chu, G. Efficient Heat Conducting Liquid Metal/CNT Pads with Thermal Interface Materials. *Bulletin of Materials Science* **2019**, *42* (4), 192. https://doi.org/10.1007/s12034-019-1872-7.

- (29) Wang, X.; Fan, L.; Zhang, J.; Sun, X.; Chang, H.; Yuan, B.; Guo, R.; Duan, M.; Liu, J. Printed Conformable Liquid Metal E-Skin-Enabled Spatiotemporally Controlled Bioelectromagnetics for Wireless Multisite Tumor Therapy. *Adv Funct Mater* **2019**, 1907063.
- (30) Kong, W.; Shah, N. U. H.; Neumann, T. v; Vong, M. H.; Kotagama, P.; Dickey, M. D.; Wang, R. Y.; Rykaczewski, K. Oxide-Mediated Mechanisms of Gallium Foam Generation and Stabilization during Shear Mixing in Air. *Soft Matter* **2020**, *16*, 5801–5805.
- (31) Zhang, M.; Liu, L.; Zhang, C.; Chang, H.; Zhang, P.; Rao, W. Self-Foaming as a Universal Route for Fabricating Liquid Metal Foams and Hollow Particles. *Adv Mater Interfaces* **2021**, 2100432.
- (32) Gao, J.; Ye, J.; Chen, S.; Gong, J.; Wang, Q.; Liu, J. Liquid Metal Foaming via Decomposition Agents. *ACS Appl Mater Interfaces* **2021**, *13* (14), 17093–17103.
- (33) Wang, H.; Yuan, B.; Liang, S.; Guo, R.; Rao, W.; Wang, X.; Chang, H.; Ding, Y.; Liu, J.; Wang, L. Plus-M: A Porous Liquid-Metal Enabled Ubiquitous Soft Material. *Mater Horiz* **2018**, *5* (2), 222–229.
- (34) Shah, N. U. H.; Kong, W.; Casey, N.; Kanetkar, S.; Wang, R. Y.-S.; Rykaczewski, K. Gallium Oxide-Stabilized Oil in Liquid Metal Emulsions. *Soft Matter* **2021**, *Advance Ar*, D1SM00982F. https://doi.org/10.1039/D1SM00982F.
- (35) Ndieguene, A.; Albert, P.; Sylvestre, J. Eternal Packages: Liquid Metal Flip Chip Devices. In *Electronic Components and Technology Conference (ECTC), 2016 IEEE 66th*; IEEE, 2016; pp 580–587.
- (36) McAfee, R.; Fish, M.; Baker, D.; Gess, J.; Boteler, L. Compatibility Analysis of Liquid Gallium and Common Packaging Metals for Application in Electronic Component Thermal Management. In 2020 19th IEEE Intersociety Conference on Thermal and Thermomechanical Phenomena in Electronic Systems (ITherm); IEEE, 2020; pp 1276–1281.
- (37) Hellebrekers, T.; Ozutemiz, K. B.; Yin, J.; Majidi, C. Liquid Metal-Microelectronics Integration for a Sensorized Soft Robot Skin. In *2018 IEEE/RSJ International Conference on Intelligent Robots and Systems (IROS)*; IEEE, 2018; pp 5924–5929.
- (38) Ozutemiz, K. B.; Wissman, J.; Ozdoganlar, O. B.; Majidi, C. EGaln–Metal Interfacing for Liquid Metal Circuitry and Microelectronics Integration. *Adv Mater Interfaces* **2018**, *5* (10), 1701596.
- (39) Doudrick, K.; Liu, S.; Mutunga, E. M. E. M.; Klein, K. L. K. L.; Damle, V.; Varanasi, K. K. K.; Rykaczewski, K. Different Shades of Oxide: From Nanoscale Wetting Mechanisms to Contact Printing of Gallium-Based Liquid Metals. *Langmuir* **2014**, *30* (23), 6867–6877. https://doi.org/10.1021/la5012023.
- (40) Politova, N.; Tcholakova, S.; Valkova, Z.; Golemanov, K.; Denkov, N. D. Self-Regulation of Foam Volume and Bubble Size during Foaming via Shear Mixing. *Colloids Surf A Physicochem Eng Asp* **2018**, *539*, 18–28.
- (41) Banhart, J. Metal Foams: Production and Stability. Adv Eng Mater 2006, 8 (9), 781–794.
- (42) Körner, C.; Arnold, M.; Singer, R. F. Metal Foam Stabilization by Oxide Network Particles. *Materials Science and Engineering: A* **2005**, *396* (1–2), 28–40.

- (43) Uppal, A.; Kong, W.; Rana, A.; Wang, R. Y.; Rykaczewski, K. Enhancing Thermal Transport in Silicone Composites via Bridging Liquid Metal Fillers with Reactive Metal Co-Fillers and Matrix Viscosity Tuning. *ACS Appl Mater Interfaces* **2021**, *13* (36), 43348–43355.
- (44) Tutika, R.; Kmiec, S.; Haque, A. B. M. T.; Martin, S. W.; Bartlett, M. D. Liquid Metal– Elastomer Soft Composites with Independently Controllable and Highly Tunable Droplet Size and Volume Loading. *ACS Appl Mater Interfaces* **2019**, *11* (19), 17873–17883. https://doi.org/10.1021/acsami.9b04569.
- (45) Bartlett, M. D.; Kazem, N.; Powell-Palm, M. J.; Huang, X.; Sun, W.; Malen, J. A.; Majidi, C. High Thermal Conductivity in Soft Elastomers with Elongated Liquid Metal Inclusions. *Proceedings of the National Academy of Sciences* **2017**, *114* (9), 2143–2148.
- (46) Mei, S.; Gao, Y.; Deng, Z.; Liu, J. Thermally Conductive and Highly Electrically Resistive Grease Through Homogeneously Dispersing Liquid Metal Droplets Inside Methyl Silicone Oil. *J Electron Packag* **2014**, *136* (1), 011009. https://doi.org/10.1115/1.4026414.
- (47) Keplinger, O.; Shevchenko, N.; Eckert, S. Visualization of Bubble Coalescence in Bubble Chains Rising in a Liquid Metal. *International Journal of Multiphase Flow* **2018**, *105*, 159–169.
- (48) Yuan, B.; Sun, X.; Wang, H.; Liu, J. Liquid Metal Bubbles. *Appl Mater Today* **2021**, *24*, 101151.
- (49) Zhao, X.; Liu, J. Liquid Metal Vacuoles. Adv Mater Interfaces 2022, 2200583.
- (50) Xiao, Y.; Ding, Y.; Lei, J.; Fu, L. Bubble-Induced In Situ Property Modulation of Liquid Metal. *Adv Mater Interfaces* **2021**, *8* (9), 2002204.
- (51) Rykaczewski, K.; Landin, T.; Walker, M. L.; Scott, J. H. J.; Varanasi, K. K. Direct Imaging of Complex Nano- to Microscale Interfaces Involving Solid, Liquid, and Gas Phases. *ACS Nano* **2012**, *6* (10). https://doi.org/10.1021/nn304250e.
- (52) Rykaczewski, K.; Anand, S.; Subramanyam, S. B. S. B.; Varanasi, K. K. Mechanism of Frost Formation on Lubricant-Impregnated Surfaces. *Langmuir* **2013**, *29* (17), 5230–5238. https://doi.org/10.1021/la400801s.
- (53) Thompson, D. R.; Rao, S. R.; Cola, B. a. A Stepped-Bar Apparatus for Thermal Resistance Measurements ¹. *J Electron Packag* **2013**, *135* (4), 041002. https://doi.org/10.1115/1.4025116.
- (54) Ralphs, M. I.; Smith, B. L.; Roberts, N. A. Technique for Direct Measurement of Thermal Conductivity of Elastomers and a Detailed Uncertainty Analysis. *Meas Sci Technol* **2016**, 27 (11), 115014. https://doi.org/10.1088/0957-0233/27/11/115014.
- (55) Ralphs, M. I. M. I.; Kemme, N.; Vartak, P. B. P. B.; Joseph, E.; Tipnis, S.; Turnage, S.; Solanki, K. N.; Wang, R. Y. R. Y. R. Y.; Rykaczewski, K. In Situ Alloying of Thermally Conductive Polymer Composites by Combining Liquid and Solid Metal Microadditives. *ACS Appl Mater Interfaces* **2018**, *10* (2), 2083–2092. https://doi.org/10.1021/acsami.7b15814.
- (56) Farrell, Z. J.; Tabor, C. Control of Gallium Oxide Growth on Liquid Metal Eutectic Gallium/Indium Nanoparticles via Thiolation. *Langmuir* **2018**, *34* (1), 234–240. https://doi.org/10.1021/acs.langmuir.7b03384.
- (57) Uppal, A.; Ralphs, M.; Kong, W.; Hart, M.; Rykaczewski, K.; Wang, R. Y. Pressure-Activated Thermal Transport via Oxide Shell Rupture in Liquid Metal Capsule Beds. *ACS Appl Mater Interfaces* **2020**, *12* (2). https://doi.org/10.1021/acsami.9b17358.

- (58) Liu, S.; Sun, X.; Kemme, N.; Damle, V. G. G.; Schott, C.; Herrmann, M.; Rykaczewski, K. Can Liquid Metal Flow in Microchannels Made of Its Own Oxide Skin? *Microfluid Nanofluidics* **2016**, *20* (1), 1–6.
- (59) Goldstein, J. I.; Newbury, D. E.; Michael, J. R.; Ritchie, N. W. M.; Scott, J. H. J.; Joy, D. C. *Scanning Electron Microscopy and X-Ray Microanalysis*; Springer, 2017.
- (60) Rajagopalan, M.; Bhatia, M. A.; Tschopp, M. A.; Srolovitz, D. J.; Solanki, K. N. Atomic-Scale Analysis of Liquid-Gallium Embrittlement of Aluminum Grain Boundaries. *Acta Mater* **2014**, *73*, 312–325.
- (61) Lyon, R. N. Liquid Metals Handbook, The Committee on the Basic Properties of Liquid Metals; 1952.

Table of Content Graphic:

